Novel Digital Cancelation Method in Presence of Harmonic Self-Interference

Hyungsik Ju, Donghyuk Gwak, Yuro Lee, and Tae-Joong Kim

In-band full-duplex (IFD) communication has recently attracted a great deal of interest because it potentially provides a two-fold spectral efficiency increase over half-duplex communications. In this paper, we propose a novel digital self-interference cancelation (DSIC) algorithm for an IFD communication system in which two nodes exchange orthogonal frequency-division multiplexing (OFDM) symbols. The proposed DSIC algorithm is based on the least-squares estimation of a self-interference (SI) channel with block processing of multiple OFDM symbols, in order to eliminate the fundamental and harmonic components of SI induced through the practical radio frequency devices of an IFD transceiver. In addition, the proposed DSIC algorithm adopts discrete Fourier transform processing of the estimated SI channel to further enhance its cancelation performance. We provide a minimum number of training symbols to estimate the SI channel effectively. The evaluation results show that our proposed DSIC algorithm outperforms a conventional algorithm.

Keywords: In-band full duplex, Digital self-interference cancelation, Orthogonal frequency-division multiplexing, Discrete Fourier transform.

I. Introduction

A conventional half duplex (HD), such as a time-division duplex (TDD) or frequency-division duplex, suffers from the degradation of the spectral efficiency because it separates the time or frequency resources for the transmission and reception of the signals. In-band full-duplex (IFD) communication, in which a communicating node transmits and receives signals in the same frequency band at the same time, has, therefore, recently attracted a great deal of interest because it potentially provides a significant increase in spectral efficiency, when compared to conventional HD communication. Due to the simultaneous transmission and reception (STR) of the signals, IFD communication utilizes time two times more efficiently than does HD, which, theoretically, results in a maximum two-fold increase in the spectral efficiency of the point-to-point (P-to-P) communication connection.

The STR feature of IFD communication can be employed not only to increase the spectral efficiency of the P-to-P connection, but also to enhance the performance of various wireless communication applications. One typical application is an IFD relay that receives a signal from the source node and simultaneously forwards the source signal to the destination node over the same frequency band [1]. In a wireless cellular network, consisting of an IFD base station (BS) supporting multiple HD users, the IFD BS is able to enhance the network throughput by transmitting a downlink signal and, at the same time, receiving an uplink signal [2]. In addition, the STR feature of IFD has been shown to be efficient for improving the performance of the medium-access control layer [3], performance of the wireless backhaul link [4], physical layer secrecy [5], and throughput of cognitive radio networks [6] and wireless-powered communication networks [7].

However, the STR feature of IFD communication causes a significant problem because the transmitted signal of an IFD

Manuscript received July 20, 2016; revised Nov. 15, 2016; accepted Feb. 2, 2017. This work was supported by the Institute for Information and Communications Technology Promotion (IITP) grant funded by the Korean government (MSIP) (No. R0101-16-244, Development of 5G Mobile Communication Technologies for Hyper-Connected Smart Services).

Hyungsik Ju (corresponding author, jugun@etri.re.kr), Donghyuk Gwak (gwakdh@etri.re.kr), Yuro Lee (yurolee@etri.re.kr), and Tae-Joong Kim (aisma@etri.re.kr) are with the 5G Giga Communication Research Laboratory, ETRI, Daejeon, Rep. of Korea.

node is received by itself and, thus, interferes with its desired received signal, which is referred to as self-interference (SI). The power of SI overwhelms that of the desired signal, as it is typically more than 100 dB larger than that of the desired signal. Therefore, SI cancelation (SIC) is a key issue for implementing IFD transceivers, and many recent studies on IFD communication have mainly focused on an efficient and effective SIC mechanism.

Thus, various SIC techniques have been proposed in the literature (for example, [8] and the references therein), which are typically based on propagation, analog, and digital domain SIC or their assorted combinations. SIC in the propagation domain, referred to as propagation SIC (PSIC), eliminates SI in the radio frequency (RF) wireless propagation channel. In addition, SIC in the analog domain, which is referred to as analog SIC (ASIC), cancels SI before the received signal is processed through analog-to-digital conversion (ADC) [9]–[11]. Finally, SIC in the digital domain, referred to as digital SIC (DSIC), eliminates the remaining SI after the ADC using digital signal processing [11]–[13]. Previously, IFD communication systems were mostly studied with the multiple antennas used in a multiple-input multiple-output (MIMO) setup to utilize PSIC, by separating the transmission and reception antennas. When compared to HD MIMO systems with the same total number of antennas, however, IFD communications with separate transmission and reception antennas do not achieve an improvement in spectral efficiency in a spatially white MIMO channel; rather, they only improve the spectral efficiency when the MIMO channel is correlated [14]. Yet, it has recently been shown that IFD transceivers can be implemented using only a single antenna and that SI of up to 110 dB higher than the noise-floor power level can be eliminated in a single-antenna IFD transceiver [13]. In addition, various negative effects of practical hardware limitations to IFD communications and SIC have been investigated, such as the harmonic components induced by the practical RF devices of the IFD transceiver [13], [15], a finite dynamic range of ADC [15], IQ imbalance [16], and SI channel estimation error [17].

Specifically, DSIC aims at eliminating the SI induced by the reflection of the transmitted signals from the air as well as that remaining after ASIC. One of the most representative DSIC schemes has been proposed in [11], which eliminates both the fundamental and harmonic components of SI based on the least-squares (LS) estimation of an SI channel, exploiting the Hammerstein model to describe the harmonic component of SI. The DSIC performance of this scheme is optimal among LS estimation-based DSIC schemes, at the expense of high computational complexity resulting from the use of a pseudo inverse of the training matrix. In [12], an iterative DSIC scheme based on the least-mean-square (LMS) algorithm has been proposed, in which the DSIC performance converges to that proposed in [11], despite its lower computational complexity. In addition, another DSIC scheme has been proposed in [13], which is based on the minimum-mean-square-error estimation of the SI channel to improve DSIC performance at the cost of exploiting the statistical information of the SI channel. Furthermore, the DSIC method proposed in [13] models the harmonic component of SI with Volterra series, and removes it utilizing the LMS algorithm. Although the Volterra model describes harmonic SI more accurately, however, it makes the computational complexity prohibitively high with marginal DSIC performance improvement, when compared to that in [11].

In this paper, we further study DSIC in IFD communication systems, in which two nodes exchange orthogonal frequency-division multiplexing (OFDM) symbols, and propose a novel DSIC algorithm. We consider OFDM a modulation scheme because currently commercialized (for example, Wi-Fi and LTE) and future wireless communication systems are deployed based on OFDM or OFDM-based multicarrier transmissions. Not to exploit the statistical a priori information of the SI channel, in addition, the proposed DSIC algorithm is based on an LS estimation of an SI channel with the block processing of multiple OFDM symbols, to eliminate both the fundamental and harmonic components of SI. In the proposed DSIC algorithm, the harmonic component of SI is described by the Hammerstein model to achieve reasonable DSIC performance with moderate complexity. Furthermore, leveraging a unique property of OFDM, our DSIC algorithm employs the discrete Fourier transform (DFT) processing of the estimated SI channel to further enhance SIC performance. Our DSIC algorithm is primarily suitable for single-antenna IFD transceivers, but can be easily generalized to multi-antenna IFD transceivers with separate transmission and reception antennas.

The rest of this paper is organized as follows. Section II presents the system model of the IFD communication with the IFD transceiver structure and general SIC procedure. Section III addresses a novel DSIC algorithm based on multi-symbol LS estimation of the SI channel. Section IV presents the evaluation results when comparing the SIC performance of the proposed DSIC algorithm with that of a conventional algorithm. Finally, Section V provides some concluding remarks.

II. System Model

In this paper, we consider IFD communication between two nodes denoted by *a* and *b*, as shown in Fig. 1. Each node has a single antenna used for the exchange of OFDM-modulated symbols through the STR in the same frequency band (in other

https://doi.org/10.4218/etrij.17.0116.0498

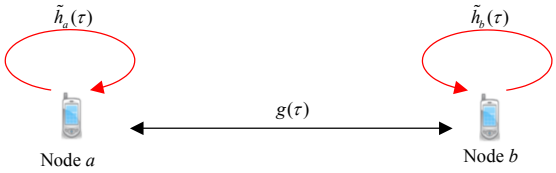

Fig. 1. Channel model of IFD communication system.

words, in-band STR). The system model in Fig. 1 describes bi-directional IFD communication between two IFD-capable communicating nodes. One typical application of this model is wireless backhaul communication between an IFD-capable macrocell base station (BS) and IFD-capable small-cell BS. Furthermore, once IFD communication becomes implementable in small IFD user equipment (UE), with the development of implementation technologies in the future, the applications of this model can be extended to bi-directional device-to-device communication between two pieces of IFD-capable UE, as well as to bi-directional IFD communication between an IFD-capable BS or access point (AP) and IFD-capable UE in cellular (for example, LTE) or Wi-Fi networks.

The in-band STR yields SI at both communicating nodes. Because both nodes have only a single antenna, the channels that the SI signals pass through (SI channels) are represented by single-input single-output (SISO) channels at both nodes. At time instant t, the impulse responses of the SI channel at nodes a and b are denoted by $\tilde{h}_a(\tau;t)$ and $\tilde{h}_b(\tau;t)$, respectively, where τ denotes the time delay at the time instant. In addition, the wireless channels from node a to node b, and from node b to node a, are also represented by SISO channels, with the impulse responses denoted by $g_{ab}(\tau;t)$ and $g_{ba}(\tau;t)$, respectively. Without a loss of generality, we assume that the channel reciprocity holds between $g_{ab}(\tau;t)$ and $g_{ba}(\tau;t)$ because the signal transmissions from (to) node a to (from) node b both occur in the same band simultaneously, and, thus, we have $g_{ab}(\tau;t) = g_{ba}(\tau;t) = g(\tau;t)$. It is further assumed that $\tilde{h}_a(\tau;t)$, $\tilde{h}_b(\tau;t)$, and $g(\tau;t)$ remain constant during the block transmission time; therefore, within this time, the time index t is later omitted, such that the aforementioned channel impulse responses are denoted as $\tilde{h}_a(\tau)$, $\tilde{h}_b(\tau)$, and $g(\tau)$, respectively.

Figure 2 shows the transceiver structure of two communicating nodes. Both the transmission and reception chains of a node are connected to a single antenna through a distributor (for example, a circulator). By employing the distributor, we typically achieve a 15-dB SI suppression. The residual SI is then eliminated in the analog and digital domains. After eliminating SI at the receiving end, the node decodes the signal transmitted by the other node.

We denote the baseband equivalent expressions of the ith and jth OFDM symbols transmitted by nodes a and b as $x_a^{(i)}(t)$ and $x_b^{(j)}(t)$, $0 \le t \le T_S$, respectively, with T_S

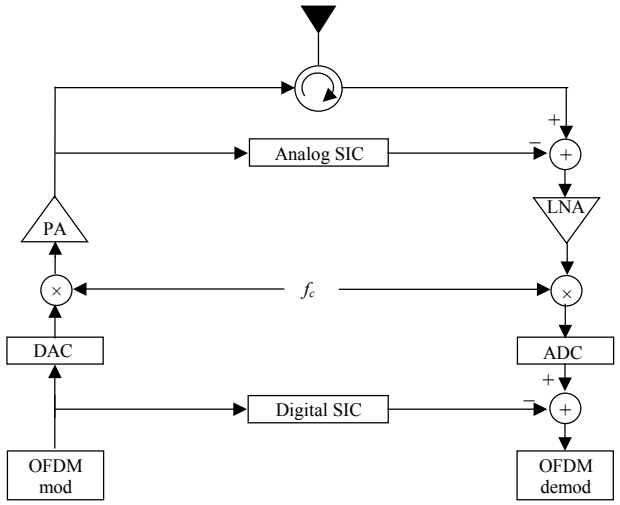

Fig. 2. Structure of IFD transceiver.

representing the OFDM symbol duration including the cyclic prefix (CP). We assume that node a transmits $x_a^{(i)}(t)$, whereas node b transmits $x_b^{(j)}(t)$. At time instant t, at which nodes a and b transmit $x_a^{(i)}(t)$ and $x_b^{(j)}(t)$, respectively, the received signal at nodes a and b can then be expressed, respectively, as:

$$\tilde{y}_a^{(i)}(t) = \left(\tilde{h}_a * x_a^{(i)}\right)(t) + \left(g * x_b^{(j)}\right)(t) + w_a^{(i)}(t), \quad (1)$$

$$\tilde{y}_b^{(j)}(t) = \left(\tilde{h}_b * x_b^{(j)}\right)(t) + \left(g * x_a^{(i)}\right)(t) + w_b^{(j)}(t), \quad (2)$$

where $w_a^{(i)}(t)$ and $w_b^{(j)}(t)$ represent the receiver noise at nodes a and b at time instant t, respectively. We assume that $w_a^{(i)}(t)$ and $w_b^{(j)}(t)$ have a zero-mean circularly symmetric complex-Gaussian distribution with $\mathrm{E}\left[\left|w_i^{(a)}(t)^2\right|\right] = \sigma_a^2$ and $\mathrm{E}\left[\left|w_i^{(b)}(t)^2\right|\right] = \sigma_b^2$, respectively. In (1), $\left(\tilde{h}_a * x_a^{(i)}\right)(t)$ and $\left(g * x_b^{(j)}\right)(t)$ represent the SI and desired signal at node a, respectively. In (2), similarly, the SI and desired signal at node b are represented by $\left(\tilde{h}_b * x_b^{(j)}\right)(t)$ and $\left(g * x_a^{(i)}\right)(t)$, respectively. We further assume that the timing offset between the receptions of the SI and desired signal at both nodes is within the CP duration. Under this assumption, we can safely transform the time-domain received signals into the equivalent frequency-domain expressions without causing inter-channel interference. Therefore, for notational brevity, we do not consider CP throughout this paper.

At node a, $x_a^{(i)}(t)$ in (1) is generated as follows. Denote the number of subcarriers in an OFDM symbol as N. The frequency-domain expression of the ith OFDM symbol transmitted by node a is then given in a vector form by:

$$\mathbf{S}_a^{(i)} = \left[S_a^{(i)}(0), \ldots, S_a^{(i)}(N-1)\right]^{\mathrm{T}}, \quad (3)$$

where $S_a^{(i)}(k)$ denotes the frequency-domain input data at the kth subcarrier, satisfying $\mathrm{E}\left[\left|S_a^{(i)}(k)^2\right|\right]=P_a$, with P_a denoting the average transmit power of node a. After an inverse discrete Fourier transform (IDFT), the time-domain expression of the ith OFDM symbol transmitted by node a is then given by:

$$\mathbf{s}_a^{(i)}=\left[s_a^{(i)}[0], \ldots, s_a^{(i)}[N-1]\right]^{\mathrm{T}}, \tag{4}$$

where:

$$s_a^{(i)}[n]=\sum_{k=0}^{N-1} S_a^{(i)}(k)e^{\frac{2\pi}{N}kn}, \quad n=0, \ldots, N-1. \tag{5}$$

After $s_a^{(i)}$ in (4) is digital-to-analog converted and then passes the RF components of the transmitting end, such as a power amplifier and local oscillator, we obtain $x_a^{(i)}(t)$ in (1). Note that the harmonics of $s_a^{(i)}$ are generated when it passes the RF components. Therefore, $x_a^{(i)}(t)$ not only contains $s_a^{(i)}$ as its fundamental component, but also contains the harmonics of $s_a^{(i)}$. Denote $T = 1/W$ as the sample period of the OFDM system, where W represents the system bandwidth. Taking the harmonics and the fundamental components into consideration, one typical way to describe $x_a^{(i)}(t)$ at a given time instant $t = nT$ is to employ a Taylor series expansion:

$$x_a^{(i)}(nT)=\sum_{m=1, m\in\text{odd}}^{M}\sqrt{\alpha_m}s_a^{(i)}[n]\left|s_a^{(i)}[n]\right|^{m-1}, \tag{6}$$

where α_m and M denote the power of the mth order harmonics and maximum order of harmonics, respectively. At node b, $x_b^{(i)}(t)$ at a time instant t within the transmission period of the jth OFDM symbol can be obtained similarly by (3) through (6) with $S_b^{(j)}=\left[S_b^{(j)}(0), \ldots, S_b^{(j)}(N-1)\right]^{\mathrm{T}}$, where $\mathrm{E}\left[\left|S_b^{(j)}(k)^2\right|\right]=P_b$.

After $\tilde{y}_a^{(i)}(t)$ in (1) is received, first, node a eliminates SI in the analog domain of the receiving end. Because node a knows $x_a^{(i)}(t)$, ASIC can be performed by estimating $\tilde{h}_a(\tau)$. Denote the estimation of $\tilde{h}_a(\tau)$ as $\hat{h}_a(\tau)$. After ASIC, $\tilde{y}_a^{(i)}(t)$ in (1) can be modified to:

$$\begin{aligned} y_a^{(i)}(t) &= \tilde{y}_a^{(i)}(t)-\left(\hat{h}_a * x_a^{(i)}\right)(t) \\ &= \left(h_a * x_a^{(i)}\right)(t)+\left(g * x_b^{(j)}\right)(t)+w_a^{(i)}(t), \end{aligned} \tag{7}$$

where $h_a(\tau)=\tilde{h}_a(\tau)-\hat{h}_a(\tau)$.

Next, $y_a^{(i)}(t)$ passes the receiver RF components, such as a low noise amplifier and local oscillator, which are then converted into digital samples. It is worth noting that the RF components of the receiving end also induce non-linear harmonics to the SI given in (7). For convenience, however, we assume that, without a loss of generality, the harmonics of SI shown in (6) already include those induced by the RF components of the receiving end. After ADC, the nth received digital sample at node a during the ith OFDM symbol transmission can be expressed as:

$$y_a^{(i)}[n]=\left(h_a * x_a^{(i)}\right)[n]+\left(g * x_b^{(j)}\right)[n]+w_a^{(i)}[n], \tag{8}$$

where $y_a^{(i)}[n]=y_a^{(i)}(nT)$ and $w_a^{(i)}[n]=w_a^{(i)}(nT)$. As will be elaborated in the next section, the proposed DSIC algorithm performs SIC in the frequency domain. By taking the DFT of $\mathbf{y}_a^{(i)}=\left[y_a^{(i)}[0], \ldots, y_a^{(i)}[N-1]\right]^{\mathrm{T}}$ with $y_i^{(a)}[n]$ given in (8), we then obtain:

$$\begin{aligned} \mathbf{Y}_a^{(i)} &= \left[Y_a^{(i)}(0), \ldots, Y_a^{(i)}(N-1)\right]^{\mathrm{T}} \\ &= \mathrm{DFT}\left(\mathbf{y}_a^{(i)}\right) \\ &= \mathbf{X}_a^{(i)}\mathbf{H}_a+\mathbf{X}_b^{(j)}\mathbf{G}+\mathbf{W}_a^{(i)}, \end{aligned} \tag{9}$$

where $\mathbf{X}_i^{(a)}$ and $\mathbf{X}_j^{(b)}$ are diagonal matrices whose diagonal entries are obtained by the DFT of $\mathbf{x}_a^{(i)}=\left[x_a^{(i)}[0], \ldots, x_a^{(i)}[N-1]\right]^{\mathrm{T}}$ with $x_a^{(i)}[n]=x_a^{(i)}(nT)$ and $\mathbf{x}_b^{(j)}=\left[x_b^{(j)}[0], \ldots, x_b^{(j)}[N-1]\right]^{\mathrm{T}}$ with $x_b^{(j)}[n]=x_b^{(j)}(nT)$, $0\le n\le N-1$, respectively. In addition, $\mathbf{H}_a=[H_a[0], \ldots, H_a[N-1]]^{\mathrm{T}}$ and $\mathbf{G}=[G[0], \ldots, G[N-1]]^{\mathrm{T}}$ represent the equivalent frequency-domain expressions of $h_a(\tau)$ and $g(\tau)$, respectively. We obtain $\mathbf{H}_a$ and $\mathbf{G}$ by the N-point DFT of $[h_a[0], \ldots, h_a[L_a-1]]^{\mathrm{T}}$ with $h_a[n]=h_a(nT)$ and $[g[0], \ldots, g[L-1]]^{\mathrm{T}}$ with $g[n]=g(nT)$, respectively, where L_a and L denote the maximum delay spread of $h_a(\tau)$ and $g(\tau)$, respectively. Finally, $\mathbf{W}_a^{(i)}=\left[W_a^{(i)}[0], \ldots, W_a^{(i)}[N-1]\right]^{\mathrm{T}}$ with $W_a^{(i)}[n]=W_a^{(i)}(nT)$, $0\le n\le N-1$, denotes the frequency-domain expression of the receiver noise at node a during the transmission time of $\mathbf{X}_a^{(i)}$. At node b, the frequency-domain received signal in the digital baseband can be equivalently obtained by (7) through (9).

III. DSIC Based on Multi-symbol LS Estimation

As shown in (9), for DSIC, we need to know which SI channels are observed in the digital domain, H_a and H_b. In this section, we propose a novel algorithm to estimate the digital domain SI channels for DSIC. The proposed algorithm, first, estimates the SI channel in the frequency domain of the digital baseband and, then, refines it to improve estimation accuracy. We begin this section by investigating the frame structure for an efficient SI channel estimation, and then elaborate on our proposed DSIC algorithm in more detail. Later in this section, we assume that ASIC has already been performed and, thus,

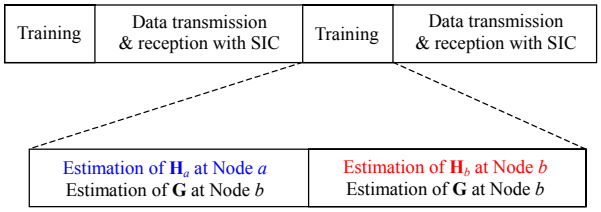

Fig. 3. Frame structure for IFD communication with SIC.

we focus only on the DSIC.

1. Frame Structure for SI Channel Estimation

Figure 3 shows the frame structure for IFD communication with SIC. The frame under consideration consists of a training field and data transmission field. During the training field, both nodes estimate channels necessary for eliminating any SI and decoding the desired signal. For this purpose, two nodes exchange known sequences (for example, preambles) before the actual exchange of their data. The data transmission field then follows at the end of training field, in which two nodes exchange their own data with IFD communication performing SIC. The estimated SI channels obtained in the training field are used for SIC in this data transmission field. The durations of one training field and one data transmission field are within a block transmission time, in which all the channels remain constant. Thus, the training field should be repeated periodically to trace the change in the SI channel between different transmission blocks.

During this training field, both nodes a and b operate with TDD, that is, node b only receives a signal, whereas node a transmits the signal in this field, and vice versa. This is because the SIC performance of a node can be degraded by its desired signal if two nodes communicate with the IFD in the training field. That is, the desired signal acts as interference, which degrades the accuracy of the SI channel estimation; an inaccurate estimation of the SI channel results in residual SI, which may severely affect the decoding of the desired signal. In general, such HD operations for estimating the SI channels in the training field are necessary not only for DSIC, but also for ASIC [9]–[13].

In the training field, for the sake of convenience, we assume that, first, node a transmits its known sequences and, then, node b transmits its known sequences after the transmission of node a is completed. We denote the frequency-domain expressions of the ith OFDM symbol transmitted by node a in the training field as $\mathbf{X}_a^{(P,i)}$. While $\mathbf{X}_a^{(P,i)}$ is being transmitted in the training field, the received signals in the baseband frequency domain at nodes a and b can be expressed by modifying (9), respectively, as:

$$\begin{aligned}\mathbf{Y}_a^{(P,i)} &= \left[Y_a^{(P,i)}(0),\ \ldots,\ Y_a^{(P,i)}(N-1)\right]^{\mathrm{T}} \\ &= \mathbf{X}_a^{(P,i)}\mathbf{H}_a + \mathbf{W}_a^{(P,i)},\end{aligned} \tag{10}$$

$$\begin{aligned}\mathbf{Y}_b^{(P,i)} &= \left[Y_b^{(P,i)}(0),\ \ldots,\ Y_b^{(P,i)}(N-1)\right]^{\mathrm{T}} \\ &= \mathbf{X}_b^{(P,i)}\mathbf{G} + \mathbf{W}_b^{(P,i)},\end{aligned} \tag{11}$$

where $\mathbf{W}_a^{(P,i)}$ and $\mathbf{W}_b^{(P,i)}$ represent the receiver noise vectors during the transmission time of $\mathbf{X}_a^{(P,i)}$ at nodes a and b, respectively. From (10) and (11), nodes a and b can estimate $\mathbf{H}_a$ and $\mathbf{G}$, respectively, because $\mathbf{X}_a^{(P,i)}$ is assumed to be a known signal at both nodes. After the transmission of node a is completed, nodes a and b can estimate $\mathbf{G}$ and $\mathbf{H}_b$, respectively, while node b transmits $\mathbf{X}_b^{(P,j)}$, denoting the frequency-domain expressions of the jth OFDM symbol transmitted by node b in the training field. An elaboration of the algorithm used to estimate $\mathbf{H}_a$ and $\mathbf{H}_b$ follows next.

2. SI Channel Estimation in Training Field

SI channel estimation in the training field is conducted, first, by estimating the SI channel based on an LS estimation utilizing multiple OFDM symbols and, then, by improving the estimation accuracy by refining the previously estimated SI channel through the DFT processing of the estimated SI channel. Figure 4 shows the procedure of the proposed SI channel estimation. Because the SI channel estimation processes at both nodes a and b are equivalent, we only consider the SI channel estimation at node a for the sake of brevity.

Denote $\mathbf{s}_a^{(P,i)}$ as the time-domain expression of the ith OFDM symbol transmitted by node a in the training field, obtained in the same way as (3) through (5). As shown in (6), $\mathbf{X}_a^{(P,i)}$ in (10) not only contains $\mathbf{s}_a^{(P,i)}$ as a fundamental

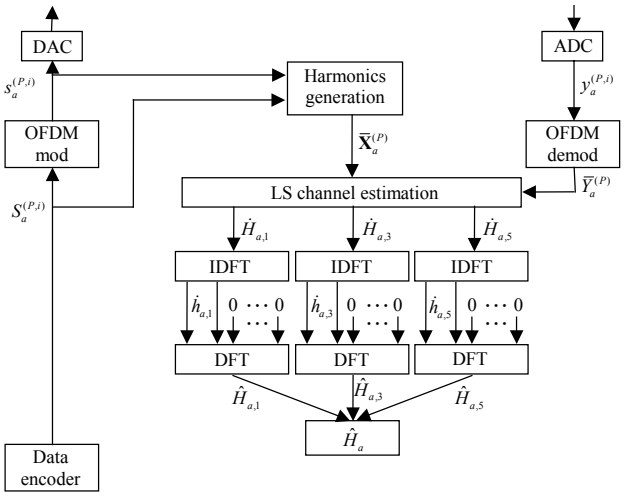

Fig. 4. SI channel estimation at node a in digital frequency domain based on multi-symbol LS estimation and DFT processing.

component, but also $\mathbf{s}_{a,m}^{(P,i)}$ as the mth order harmonics, $m = 1, 3, \ldots, M$, where $\mathbf{s}_{a,m}^{(P,i)} = \left[s_{a,m}^{(P,i)}[0], \ldots, s_{a,m}^{(P,i)}[N-1] \right]^{\mathrm{T}}$ with $s_{a,m}^{(P,i)}[n] = s_a^{(P,i)}[n] \left| s_a^{(P,i)}[n] \right|^{m-1}$, $N = 0, \ldots, N-1$. To take the harmonic components into consideration, therefore, we can alternatively express $\mathbf{Y}_a^{(P,i)}$ in (10) based on (6), as:

$$\mathbf{Y}_a^{(P,i)} = \sum_{m=\text{odd}}^{M} \overline{\mathbf{X}}_{a,m}^{(P,i)} \overline{\mathbf{H}}_{a,m} + \mathbf{W}_a^{(P,i)}, \tag{12}$$

$$= \overline{\mathbf{X}}_a^{(P,i)} \overline{\mathbf{H}}_a + \mathbf{W}_a^{(P,i)}, \tag{13}$$

where M is an odd number representing the maximum order of harmonic components under consideration. In addition, $\overline{\mathbf{X}}_a^{(P,i)} = \left[\overline{\mathbf{X}}_{a,1}^{(P,i)}, \overline{\mathbf{X}}_{a,3}^{(P,i)}, \ldots, \overline{\mathbf{X}}_{a,M}^{(P,i)} \right]$ corresponds to the frequency-domain expression of the ith OFDM symbol of node a with harmonics transmitted in the training field, where $\overline{\mathbf{X}}_{a,m}^{(P,i)}$ is a diagonal matrix whose diagonal entries consists of the frequency-domain expressions of $s_a^{(P,i)}[n] \left| s_a^{(P,i)}[n] \right|^{m-1}$, $n = 0, \ldots, N-1$. The kth diagonal entry of $\overline{\mathbf{X}}_{a,m}^{(P,i)}$ is, thus, given by:

$$\overline{X}_{a,m}^{(P,i)}(k) = \sum_{n=0}^{N-1} s_a^{(P,i)}[n] \left| s_a^{(P,i)}[n] \right|^{m-1} e^{-j\frac{2\pi}{N}nk}. \tag{14}$$

By adopting $\overline{\mathbf{X}}_{a,m}^{(P,i)}$ in (14), $\mathbf{H}_a$ in (10) is replaced by $\overline{\mathbf{H}}_a = \left[\overline{\mathbf{H}}_{a,1}^{\mathrm{T}} \overline{\mathbf{H}}_{a,3}^{\mathrm{T}} \cdots \overline{\mathbf{H}}_{a,M}^{\mathrm{T}} \right]^{\mathrm{T}}$, with $\overline{\mathbf{H}}_{a,m} = \left[\overline{\mathbf{H}}_{a,m}(0) \cdots \overline{\mathbf{H}}_{a,m}(N-1) \right]^{\mathrm{T}}$, $m = 1, 3, \ldots, M$, denoting the frequency-domain expression of the SI channel through which the mth harmonic component (that is, $s_a^{(P,i)}[n] \left| s_a^{(P,i)}[n] \right|^{m-1}$) passes. As opposed to (10), in which the SI channel is treated as a single variable, the SI channels through which different orders of harmonics pass are treated by different variables in (13).

Because $\overline{\mathbf{X}}_{a,1}^{(P,i)}$, $\overline{\mathbf{X}}_{a,3}^{(P,i)}, \ldots, \overline{\mathbf{X}}_{a,M}^{(P,i)}$ and, thus, $\overline{\mathbf{X}}_a^{(P,i)}$ are all known matrices, (13) is equivalent to a linear equation through which we should obtain the solutions of the variables in $\overline{\mathbf{H}}_a$ from the given $\mathbf{Y}_a^{(P,i)}$. Note, however, that (13) is an underdetermined system because we have to estimate multiple variables in $\overline{\mathbf{H}}_a$ (that is, $\overline{\mathbf{H}}_{a,1}, \overline{\mathbf{H}}_{a,3}, \ldots, \overline{\mathbf{H}}_{a,M}$) from a single observation $\mathbf{Y}_a^{(P,i)}$. Therefore, we cannot obtain a unique $\overline{\mathbf{H}}_a$ using (13). To tackle this problem, we use Q OFDM symbols processed together. Then, (13) can be modified as:

$$\overline{\mathbf{Y}}_a^{(P)} = \overline{\mathbf{X}}_a^{(P)} \overline{\mathbf{H}}_a + \overline{\mathbf{W}}_a^{(P)}, \tag{15}$$

where $\overline{\mathbf{X}}_a^{(P)}, \overline{\mathbf{Y}}_a^{(P)}$, and $\overline{\mathbf{W}}_a^{(P)}$ are given, respectively, by:

$$\overline{\mathbf{X}}_a^{(P)} = \begin{bmatrix} \overline{\mathbf{X}}_{a,1}^{(P,1)} & \overline{\mathbf{X}}_{a,3}^{(P,1)} & \cdots & \overline{\mathbf{X}}_{a,M}^{(P,1)} \\ \overline{\mathbf{X}}_{a,1}^{(P,2)} & \overline{\mathbf{X}}_{a,3}^{(P,2)} & \cdots & \overline{\mathbf{X}}_{a,M}^{(P,2)} \\ \vdots & \vdots & \ddots & \vdots \\ \overline{\mathbf{X}}_{a,1}^{(P,Q)} & \overline{\mathbf{X}}_{a,3}^{(P,Q)} & \cdots & \overline{\mathbf{X}}_{a,M}^{(P,Q)} \end{bmatrix}, \tag{16}$$

$$\overline{\mathbf{Y}}_a^{(P)} = \left[\left(\mathbf{Y}_a^{(P,1)} \right)^{\mathrm{T}} \left(\mathbf{Y}_a^{(P,2)} \right)^{\mathrm{T}} \cdots \left(\mathbf{Y}_a^{(P,Q)} \right)^{\mathrm{T}} \right]^{\mathrm{T}}, \tag{17}$$

$$\overline{\mathbf{W}}_a^{(P)} = \left[\left(\overline{\mathbf{W}}_a^{(P,1)} \right)^{\mathrm{T}} \left(\overline{\mathbf{W}}_a^{(P,2)} \right)^{\mathrm{T}} \cdots \left(\overline{\mathbf{W}}_a^{(P,Q)} \right)^{\mathrm{T}} \right]^{\mathrm{T}}. \tag{18}$$

By utilizing multiple OFDM symbols, the linear equation in (15) now obtains solutions of $(M+1)/2$ variables from Q given observations (that is, $\mathbf{Y}_a^{(P,1)}, \mathbf{Y}_a^{(P,2)}, \ldots, \mathbf{Y}_a^{(P,Q)}$). Therefore, we can estimate $\overline{\mathbf{H}}_a$ from (14) provided that Q is larger than or equal to the number of harmonic orders under consideration, that is:

$$Q \geq (M+1)/2. \tag{19}$$

The length of the training field at each node can, thus, be determined as Q OFDM symbols. Provided that (19) holds, the LS estimation of $\overline{\mathbf{H}}_a$, denoted by $\dot{\mathbf{H}}_a$, is given from (15) by:

$$\dot{\mathbf{H}}_a = \left(\left(\overline{\mathbf{X}}_a^{(P)} \right)^{\mathrm{H}} \overline{\mathbf{X}}_a^{(P)} \right)^{-1} \left(\overline{\mathbf{X}}_a^{(P)} \right)^{\mathrm{H}} \overline{\mathbf{Y}}_a^{(P)}, \tag{20}$$

where $\mathbf{X}^{\mathrm{H}}$ represents the Hermitian matrix of matrix $\mathbf{X}$.

The estimated frequency domain SI channel in (20) contains receiver noise spread over the entire bandwidth. It is worth noting that without loss of generality, the maximum delay spread of the SI channel can be assumed to be shorter than the CP duration. In the time domain-equivalent form of (20), therefore, all information about the SI channel is contained in the first few samples, whereas other samples contain receiver noise only. By removing such noise, which is enabled by exploiting the time-frequency conversion property of the OFDM system yielded by DFT, we can reduce the power of the receiver noise over the entire bandwidth, resulting in enhanced SI-channel estimation accuracy. From (15) and (20), the estimated frequency-domain SI channel $\dot{\mathbf{H}}_a$ can be alternatively expressed as:

$$\dot{\mathbf{H}}_a = \overline{\mathbf{H}}_a + \dot{\boldsymbol{\varepsilon}}_a, \tag{21}$$

where $\dot{\boldsymbol{\varepsilon}}_a$ denotes the channel estimation error induced by the receiver noise, given by:

$$\begin{aligned} \dot{\boldsymbol{\varepsilon}}_a &= \left[\dot{\boldsymbol{\varepsilon}}_{a,1}^{\mathrm{T}} \ \dot{\boldsymbol{\varepsilon}}_{a,3}^{\mathrm{T}} \ \cdots \ \dot{\boldsymbol{\varepsilon}}_{a,M}^{\mathrm{T}} \right] \\ &= \left(\left(\overline{\mathbf{X}}_a^{(P)} \right)^{\mathrm{H}} \overline{\mathbf{X}}_a^{(P)} \right)^{-1} \left(\overline{\mathbf{X}}_a^{(P)} \right)^{\mathrm{H}} \overline{W}_a^{(P)}, \end{aligned} \tag{22}$$

with $\dot{\boldsymbol{\varepsilon}}_{a,m} = \left[\dot{\varepsilon}_{a,m}(0), \ldots, \dot{\varepsilon}_{a,m}(N-1) \right]^{\mathrm{T}}$ corresponding to the error with respect to estimating $\dot{\mathbf{H}}_{a,m}$. Recall that $\dot{\mathbf{H}}_a$ consists of the estimated SI channels with different orders, that is, $\dot{\mathbf{H}}_{a,m}$, $m = 1, 3, \ldots, M$, each of which is obtained from independently designed $\overline{\mathbf{X}}_{a,m}^{(P,i)}$ in (14). Therefore, we should take the DFT process of individual $\dot{\mathbf{H}}_{a,m}$ independently. We denote the IDFT of $\dot{\mathbf{H}}_{a,m}$ as:

https://doi.org/10.4218/etrij.17.0116.0498

$$\dot{\mathbf{h}}_{a,m} = \left[\dot{h}_{a,m}[0], \ldots, \dot{h}_{a,m}[N-1]\right]^{\mathrm{T}}, \quad (23)$$

with $\dot{h}_{a,m}[n]$, $m = 1, 3, \ldots, M$, given by:

$$\dot{h}_{a,m}[n] = \sum_{k=0}^{N-1} \dot{H}_{a,m}(k) e^{-j\frac{2\pi}{N}kn}, \quad 0 \le n \le N-1. \quad (24)$$

Note that $\dot{h}_{a,m}[n]$ with $n \ge L_a$ has receiver noise only [18]. Therefore, we can reduce the effect of the receiver noise by forcing zeros to $\dot{h}_{a,m}[n]$ with $n \ge L_a$, as follows.

$$\hat{h}_{a,m}[n] = \begin{cases} \dot{h}_{a,m}[n], & 0 \le n \le L_a - 1, \\ 0, & L_a \le n \le N-1, \end{cases} \quad m = 1, 3, \ldots, M. \quad (25)$$

The estimated SI channel in the frequency domain is then obtained by Ĥa $\hat{\mathbf{H}}_a = \left[\hat{\mathbf{H}}_{a,1}^{\mathrm{T}}, \hat{\mathbf{H}}_{a,3}^{\mathrm{T}}, \ldots, \hat{\mathbf{H}}_{a,M}^{\mathrm{T}}\right]^{\mathrm{T}}$, where $\hat{\mathbf{H}}_{a,m}$ is given by $\hat{\mathbf{H}}_{a,m} = [\hat{H}_{a,m}(0), \ldots, \hat{H}_{a,m}(N-1)]^{\mathrm{T}}$ with:

$$\hat{H}_{a,m}(k) = \sum_{k=0}^{N-1} \hat{h}_{a,m}[n] e^{j\frac{2\pi}{N}nk}, \quad 0 \le k \le N-1. \quad (26)$$

From (25) and (26), $\hat{\mathbf{H}}_a$ can be expressed as:

$$\hat{\mathbf{H}}_a = \bar{\mathbf{H}}_a + \hat{\boldsymbol{\varepsilon}}_a, \quad (27)$$

where the error covariance matrix with respect to $\hat{\boldsymbol{\varepsilon}}_a$ is given from [18] by:

$$\mathrm{E}\left[\hat{\boldsymbol{\varepsilon}}_a \hat{\boldsymbol{\varepsilon}}_a^{\mathrm{H}}\right] = \frac{L_a \sigma_a^2}{N} \mathrm{E}\left[\left(\left(\bar{\mathbf{X}}_a^{(P)}\right)^{\mathrm{H}} \bar{\mathbf{X}}_a^{(P)}\right)^{-\mathrm{H}}\right]. \quad (28)$$

Figure 5 compares the relative amplitude of $\dot{\mathbf{H}}_a$ and $\hat{\mathbf{H}}_a$ over $\mathbf{H}_a$ with $N = 64$, $M = 5$, and $Q = 3$ for a given realization of $\mathbf{H}_a$. Among 64 subcarriers, 12 are set to be null, as in a typical Wi-Fi system. Furthermore, it is assumed that α_1, α_3, and α_5 in (6) are 50 dB, 20 dB, and 0 dB larger than σ_a^2,

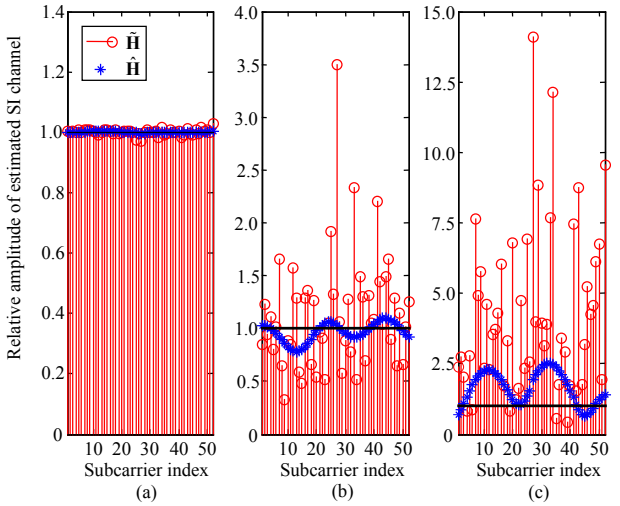

Fig. 5. Relative amplitude of estimated SI channel for (a) fundamental, (b) third order harmonic, and (c) fifth order harmonic components.

respectively. In Fig. 5, the SI channel estimation is more accurate as the relative amplitudes of the subcarriers move closer to 1. As shown in this figure, the estimation of the SI channel is more accurate with a smaller m. This is because, with a smaller value of m, we have a larger value of α_m and, thus, the corresponding signal-to-noise ratio (SNR) becomes larger. On the other hand, the DFT processing of the estimated SI channel in (24) through (26) is more effective with a larger m because the amount of reduced noise power becomes more substantial.

3. SIC in Data Transmission Field

In the data transmission field, nodes a and b exchange their data with IFD communication, conducting DSIC using their respective estimated SI channels obtained in the training field. Denote the ith OFDM symbol transmitted by node a and the jth OFDM symbol transmitted by node b as $\mathbf{X}_a^{(D,i)}$ and $\mathbf{X}_b^{(D,j)}$, respectively. Based on (9), (10), and (13), the received signal at node a during the transmission time of $\mathbf{X}_a^{(D,i)}$ can be expressed as:

$$\begin{aligned} \mathbf{Y}_a^{(D,i)} &= \left[Y_a^{(D,i)}(0), \ldots, Y_a^{(D,i)}(N-1)\right]^{\mathrm{T}} \\ &= \bar{\mathbf{X}}_a^{(D,i)} \bar{\mathbf{H}}_a + \mathbf{X}_b^{(D,j)} \mathbf{G} + \mathbf{W}_a^{(D,i)}, \end{aligned} \quad (29)$$

where $\bar{\mathbf{X}}_a^{(D,i)}$ represents the extension of $\mathbf{X}_a^{(D,i)}$ in the same way as in (12) and (13). In addition, $\mathbf{W}_a^{(D,i)}$ denotes the receiver noise at node a during the transmission time of $\mathbf{X}_a^{(\mathrm{D},i)}$. From (27), the DSIC conducted at node a can be expressed as:

$$\mathbf{Y}_a^{(D,i)} - \bar{\mathbf{X}}_a^{(D,i)} \hat{\mathbf{H}}_a = \mathbf{X}_b^{(D,j)} \mathbf{G} + \hat{\mathbf{W}}_a^{(D,i)}, \quad (30)$$

where $\hat{\mathbf{W}}_a^{(D,i)}$ represents the residual SI plus receiver noise after the DSIC, which is given by:

$$\hat{\mathbf{W}}_a^{(D,i)} = \mathbf{W}_a^{(D,i)} + \bar{\mathbf{X}}_a^{(D,i)} \hat{\boldsymbol{\varepsilon}}_a. \quad (31)$$

From (28) and (31), the covariance matrix of $\hat{\mathbf{W}}_a^{(D,i)}$ can be attained as:

$$\begin{aligned} \boldsymbol{\Phi}_{\hat{\varepsilon}_a} &= \mathrm{E}\left[\hat{\boldsymbol{\varepsilon}}_a \hat{\boldsymbol{\varepsilon}}_a^{\mathrm{T}}\right] \\ &= \sigma_a^2 \mathbf{I} + \frac{L_a \sigma_a^2}{N} \mathrm{E}\left[\bar{\mathbf{X}}_a^{(D,i)} \left(\left(\bar{\mathbf{X}}_a^{(P)}\right)^{\mathrm{H}} \bar{\mathbf{X}}_a^{(P)}\right)^{-\mathrm{H}} \left(\bar{\mathbf{X}}_a^{(D,i)}\right)^{\mathrm{H}}\right]. \end{aligned} \quad (32)$$

From (13) and (16), it can be inferred that $\boldsymbol{\Phi}_{\hat{\varepsilon}_a}$ is not a diagonal matrix because the fundamental and harmonic components in both $\bar{\mathbf{X}}_a^{(P)}$ and $\bar{\mathbf{X}}_a^{(D,i)}$ are not independent of one another. Therefore, we can conclude that our proposed DSIC algorithm causes colored noise after the DSIC.

Although the proposed DSIC algorithm is described based on bi-directional communication between two IFD nodes, it can be easily applied to uni-directional IFD communication, in which one IFD node transmits (receives) signals to (from) two

HD nodes over the same frequency band simultaneously. In this case, assuming node a is the IFD-capable node, the frame structure in Fig. 3 requires only the training period for estimating $\mathbf{H}_a$ at node a, and that for estimating $\mathbf{H}_b$ at node b is omitted from the frame. The HD node receiving signals from the IFD node a estimates $\mathbf{G}$ (the wireless channel for downlink transmission), while node a estimates $\mathbf{H}_a$. The procedures with which node a estimates the SI channel are exactly the same as those in (12) through (27). A typical application of this model is cellular or Wi-Fi networks, in which an IFD BS (or AP) supports two or more pieces of HD UE for simultaneous uplink and downlink transmissions. Furthermore, a simultaneous data reception-jamming transmission system [5] and IFD wireless-powered communication network [7] are special cases of such a model.

IV. Simulation Results

In this section, we compare the performance of the proposed DSIC algorithm with that of the conventional one in [11], which sequentially eliminates SI from the smaller-order harmonics. We conducted our simulations in an IEEE 802.11g Wi-Fi environment. The detailed simulation parameters are summarized in Table 1. To focus on the DSIC, we assume an ideal ASIC that reduces the SI power without causing any distortion of the desired signal or receiver noise.

For the purpose of exposition, ASIC gain is furthermore taken into consideration by assuming that the SI channels after the ASIC observed in the baseband digital domain (that is, $\mathbf{H}_a$ and $\mathbf{H}_b$) are given with $H_a(k) = H_b(k) = 110 - \gamma$ dB, $k = 0, 1, \ldots, N-1$, where γ denotes the ASIC gain. Moreover, $\mathbf{G}$ is also assumed to be an additive white Gaussian noise channel, in which $G(k) = \delta$, $k = 0, 1, \ldots, N-1$, where δ denotes the signal power attenuation by the distance-dependent path loss.

Figure 6 shows the uncoded bit-error rate (BER) performances of the proposed DSIC and conventional algorithms after the DSIC is applied, with respect to the different values of the average received SNR of the desired signal given by:

$$\rho = P_a \delta / \sigma_a^2 = P_b \delta / \sigma_b^2. \quad (33)$$

It can be seen in this figure that the BER of the proposed DSIC algorithm decreases with an increasing ρ, whereas that of the conventional algorithm converges to a certain value when ρ is larger than a certain threshold. In addition, the BER of the proposed DSIC algorithm was observed to converge with the ASIC gain at $\gamma \geq 40$ dB, whereas that of the conventional algorithm significantly depends on the value of γ.

Next, Fig. 7 shows the uncoded BER of the proposed and conventional DSIC algorithms with respect to the different values of ASIC gain γ. For both DSIC algorithms, the minimum ASIC gain required for the minimum value of the BER to converge decreases as the received SNR of the desired signal ρ increases. It was observed that the proposed DSIC algorithm outperforms the conventional version when ρ = 30 dB. Moreover, the proposed algorithm outperforms the conventional algorithm with $\gamma < 72$ dB and $\gamma < 68$ dB when ρ = 15 dB and ρ = 21 dB, respectively. In addition, the minimum ASIC gains required for the BER to converge are observed to be 30 dB to 40 dB and 70 dB to 80 dB for the proposed and conventional DSIC algorithms, respectively. With our proposed algorithm, therefore, it can be inferred that the requirement for designing the ASIC mechanism becomes less strict because our proposed DSIC algorithm is more tolerant to the variation of ASIC performance.

Table 1. Simulation parameters.

Parameters		Value
Bandwidth		20 MHz
Carrier frequency		2.4 GHz
Number of subcarriers (N)		64
Number of null subcarriers		12
Transmit power ($P_a = P_b$)		20 dBm
Noise floor ($\sigma_a^2 = \sigma_b^2$)		–90 dBm
Maximum order of harmonic (M)		5
Power of harmonics	Fundamental	$\alpha_1 = 0$ dB
	3rd order	$\alpha_3 = -30$ dB
	5th order	$\alpha_5 = -50$ dB
Length of training filed (Q)		3 OFDM symbols
Length of data		200 bytes
Modulation		Quadrature phase shift keying

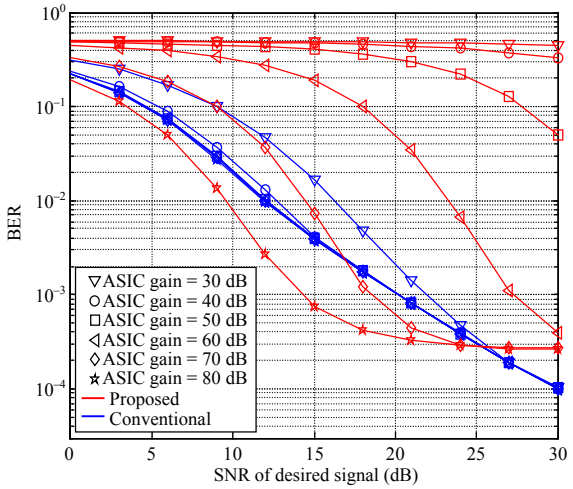

Fig. 6. Bit-error rate of conventional versus proposed DSIC algorithms according to SNR of desired signal.

ETRI Journal, Volume 39, Number 2, April 2017
https://doi.org/10.4218/etrij.17.0116.0498

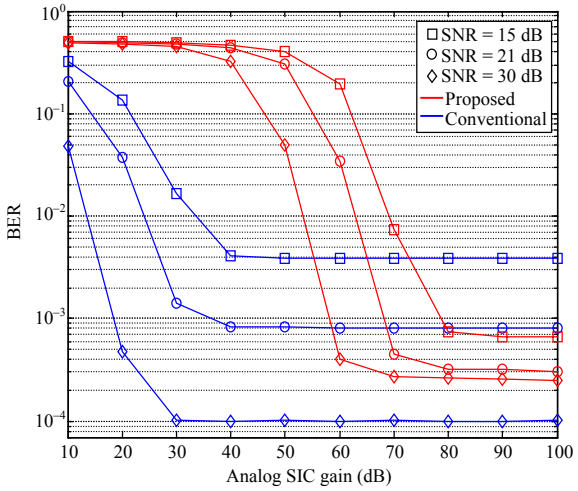

Fig. 7. Bit-error rate of conventional versus proposed DSIC algorithms according to SNR of desired signal.

It is worth noting that, as shown in Figs. 6 and 7, the proposed algorithm improves DSIC performance in the practical ranges of ASIC gains, when compared to the conventional version. For the IFD transceiver structure with a shared antenna, as shown in Fig. 2, ASIC gain achievable by distributor and analog finite impulse response filters typically range from 50 dB to 60 dB in practice [8]–[10]. Although the conventional scheme can outperform our proposed algorithm when ASIC gain is larger than 70 dB, such an ASIC gain is, in general, not achievable in practice. Furthermore, the proposed DSIC algorithm is more beneficial as the received SNR of the desired signal increases because its BER performance decreases unbounded with the increasing SNR of the received desired signal, whereas that of the conventional scheme is bounded, as observed in Figs. 6 and 7. Thus, we can conclude that our proposed algorithm is more suitable for efficient IFD communication in practice. In particular, the proposed algorithm is more beneficial for supporting UE in a cell-center area or small-cell environment where the SNR of the desired signal is sufficiently high.

V. Conclusion

In this paper, we proposed a novel DSIC algorithm that eliminates both the fundamental and harmonic components of SI. To do so, the proposed DSIC algorithm estimates the SI channel based on LS estimation with multiple OFDM symbols in the frequency domain. In addition, we effectively provided the minimum number of training symbols required to the SI channel. SI channel estimation is further refined through the DFT processing of the estimated SI channel to enhance SIC performance. Through simulations, it was shown that our proposed DSIC algorithm outperforms the conventional version by efficiently reducing the residual SI after the SIC is completed.

References

[1] H. Ju, E. Oh, and D. Hong, "Improving Efficiency of Resource Usage in Two-Hop Full Duplex Relay Systems Based on Resource Sharing and Interference Cancellation," *IEEE Trans. Wireless Commun.*, vol. 8, no. 8, Aug. 2009, pp. 3933–3938.

[2] S. Goyal et al., "Full Duplex Cellular System: Will Doubling Interference Prevent Doubling Capacity?," *IEEE Commun. Mag.*, vol. 53, no. 5, May 2015, pp. 121–127.

[3] K.M. Thilina et al., "Medium Access Control Design for Full Duplex Wireless Systems: Challenges and Approaches," *IEEE Commun. Mag.*, vol. 53, no. 5, May 2015, pp. 112–120.

[4] H. Tabassu, A.H. Sakr, and E. Hossain, "Analysis of Massive MIMO-Enabled Downlink Wireless Backhauling for Full-Duplex Small Cells," *IEEE Trans. Commun.*, vol. 64, no. 6, June 2016, pp. 2354–2369.

[5] F. Zhu et al., "Physical-Layer Security for Full Duplex Communication with Self-Interference Mitigation," *IEEE Trans. Wireless Commun.*, vol. 15, no. 1, Jan. 2016, pp. 329–340.

[6] J. Heo et al., "Simultaneous Sensing and Transmission in Cognitive Radio," *IEEE Trans. Wireless Commun.*, vol. 13, no. 4, Apr. 2014, pp. 1948–1959.

[7] H. Ju and R. Zhang, "Optimal Resource Allocation in Full-Duplex Wireless Powered Communication Networks," *IEEE Trans. Commun.*, vol. 62, no. 10, Oct. 2014, pp. 3528–2540.

[8] D. Kim et al., "A Survey of In-band Full-Duplex Transmission: from the Perspective of PHY and MAC Layers," *IEEE Commun. Survey Tutorials*, vol. 17, no. 4, Oct. 2015, pp. 2017–2046.

[9] T. Chen et al., "A Multi-stage Self-Interference Canceller for Full-Duplex Wireless Communications," *IEEE Global Commun. Conf.*, San Diego, CA, USA, Dec. 6–10, 2015, pp. 1–5.

[10] K.E. Kolodziej, J.G. McMichael, and B.T. Perry, "Multitap RF Canceller for In-band Full-Duplex Wireless Communications," *IEEE Trans. Wireless Commun.*, vol. 15, no. 6, June 2016, pp. 4321–4334.

[11] D. Bharadia et al., "Full Duplex Radios," *Proc. ACM SIGCOMM Conf.*, Hong Kong, China, Aug. 12–16, 2013, pp. 375–386.

[12] V. Tapio and M. Sonkki, "Analog and Digital Self-Interference Cancellation for Full-Duplex Transceivers," *Eur. Wireless Conf.*, Oulu, Finland, May 18–20, 2016, pp. 1–5.

[13] J. Liu et al., "Digital Nonlinear Self-Interference Cancellation Based on LMS-Volterra Algorithm," *Int. Conf. Inform. Sci. Eng.*, Beijing, China, July 8–10, 2016, pp. 1298–1302.

[14] H. Ju et al., "Bi-Directional Use of Spatial Resources and Effects of Spatial Correlation," *IEEE Trans. Wireless Commun.*, vol. 10, no. 20, Oct. 2011, pp. 3368–3379.

[15] D. Korpi et al., "Full-Duplex Transceiver System Calculations:

Analysis of ADC and Linearity Challenges," *IEEE Trans. Wireless Commun.*, vol. 13, no. 7, July 2014, pp. 3821–3836.

[16] M. Sakai et al., "Self-Interference Cancellation in Full-Duplex Wireless with IQ Imbalance," *Phy. Commun.*, vol. 18, no. 1, Mar. 2016, pp. 2–14.

[17] D. Kim et al., "Effects of Channel Estimation Error on Full-Duplex Two-Way Networks," *IEEE Trans. Veh. Technol*., vol. 62, no. 9, Nov. 2013, pp. 4666–4672.

[18] Y. Kang, K. Kim, and H. Park, "Efficient DFT-Based Channel Estimation for OFDM Systems on Multipath Channels," *IET Commun.*, vol. 1, no. 2, Apr. 2007, pp. 197–202.

Hyungsik Ju received his BS and PhD degrees in electrical engineering from Yonsei University, Seoul, Rep. of Korea, in 2005 and 2011, respectively. From Sept. 2011 to Mar. 2012, he worked as a Researcher at Yonsei University. From Mar. 2012 to Aug. 2014, he was with the Department of Electrical and Computer Engineering of the National University of Singapore, as a research fellow. Since Sept. 2014, he has been with the ETRI, Daejeon, Rep. of Korea, as a senior researcher. His current research interests include full-duplex wireless communication, wireless information and power transfer, wireless-powered networks, relay-based multi-hop communication, and full-duplex relay systems.

Donghyuk Gwak received his BS and MS degrees in electrical engineering from Seoul National University, Rep. of Korea, in 2010 and 2013, respectively. Since 2013, he has been a researcher with the ETRI, Daejeon, Rep. of Korea. His interests include beamforming, interference management, compressive sensing, and massive MIMO.

Yuro Lee received his BS and MS degrees in electrical engineering from Seoul City University, Rep. of Korea, in 1997 and 1999, respectively. Since 2001, he has been with the ETRI, Daejeon, Rep. of Korea, where he is currently a principal research engineer. His current research interests are broadband wireless transmission technologies and 5G mobile communications.

Tae-Joong Kim received his BS, MS, and PhD degrees from Yonsei University, Seoul, Rep. of Korea, in 1991, 1993, and 1998, respectively. From 1998 to 2000, he was a senior researcher of the ETRI, Daejeon, Rep. of Korea. He joined with Econex Ltd., Pyeongtaek, Rep. of Korea in 2001, where he worked, first, in chipset system design and, later, in software protocol stacking and field testing, until 2006. He returned to the ETRI in 2006, and developed a 4G-LTE, 5G mobile communication system, and is currently the managing director of the Mobile Transmission Research Department there, managing some 5G projects sponsored by the government.